Boundary effect on the spontaneous deformation of a liquid crystal elastomer plate with arbitrary director orientation

Ying Liu ●[*] and Dong Zhao
School of Civil Engineering, Beijing Jiaotong University, Beijing 100044 China

Except for director orientation, the deformation modes of constrained liquid crystal elastomer thin plate display specimen geometry size dependence due to the boundary effect. In this paper, the effect of plate geometry size on the spontaneous deformation of a simply supported liquid crystal elastomer plate is studied. The relation between the deformation modes with director orientation and plate geometry size are investigated. Results show that the deformation modes are decided by the director orientation for a certain liquid crystal elastomer, but the geometry size affects the mode transformation with respect to the director. These results are supposed to be used in the design and application of liquid crystal elastomer-based smart actuators or sensors.

I. INTRODUCTION

Smart soft actuators, that exhibit programmable, fast, and reversible shape variation under various kinds of external stimuli, have attracted more and more academic intention [1–3] considering their potential values in soft robots [4], artificial muscle [5], wearable electronics [6], and so on. Among the general stimuli including the thermal, electric, light, magnetic, or solvent one [7–10], the light shows advantage due to its easy and precise controlling in noncontact and a remote way [11]. Therefore, programming the photoresponsive material to achieve multiple desired deformations is an interesting and prospective aspect in the smart device design.

Among the various photoresponsive materials, liquid crystal elastomer (LCE) is supposed to be one of the ideal materials. Structurally, LCE is weakly cross-linked polymer with liquid crystal moiety, which possesses both the anisotropic orientation order of liquid crystal and the elasticity of polymer networks [12]. Thanks to the liquid crystal molecules, liquid crystal elastomer possesses stimuli-responsive and reversible shape variation at the macroscopic scale [13]. Considering the novel responses of LCE under light stimuli, exploring the method for precise control of LCE structures and obtaining the desired photo actuation mode become more and more attractive [14–16].

The spontaneous deformation of LCE has been experimentally demonstrated [17–19]. Meanwhile, the curvatures of LCE plates with uniform director field have been investigated theoretically, showing that the spontaneous bending could be obtained and the flat surface could even transform into a surface with Gaussian curvature [20–23]. Some research showed that the Gaussian curvature of a LCE thin sheet could be programmed by designing the in-plane director distribution including the planar nematic [24–26], splay or twist nematic [27,28], and spiral patterns [29,30]. It is seen that for LCE beam structures, the director was mainly uniformly distributed along the beam axis [31–34], and for the platelike LCE structures, the director was ordinarily treated as a planar distribution [28,35]. However, in the real application, the director is three-dimensional orientated and the specimen is ordinarily constrained. Zhao and Liu [36] analyzed the spontaneous bending of simply supported rectangular LCE plates, and established the relation between the deformation modes and director orientation. It is noticed that for a constrained LCE plate, the deformation mode transformation along with the director relies on the plate dimension. Since the specimen size could be arbitrary and usually constrained, clarification of the plate geometrical size on the bending modes of the LCE plate is necessary for its further application in smart devices, which unfortunately has been less focused.

Aiming at these problems, in this paper the effect of the plate size on the spontaneous deformation of a simply supported LCE thin plate is studied to clarify the boundary effect. Firstly, by using the finite-difference method, the spontaneous deformation of the simply supported LCE plate is delineated. Then different director orientation and plate dimension ratio are taken into consideration to clarify the dependence of the deformation pattern transformation with the director on the geometrical size of the plate. Finally, the conclusion is given.

II. GOVERNING EQUATION FOR THE SPONTANEOUS DEFORMATION OF LCE PLATE

As shown in Fig. 1, a simply supported LCE plate is perpendicularly illuminated by light with the uniform light intensity I_0. The length of the rectangular LCE plate is a, width $b = \zeta a$, and thickness h. Because the plate is always treated as a one-way plate while ζ is small, the parameter ζ changes from 0.4 to 1 to obtain an arbitrary LCE plate.

According to our previous work [36], based on the Kirchhoff-Love thin-plate theory, the dimensionless

----
*yliu5@bjtu.edu.cn
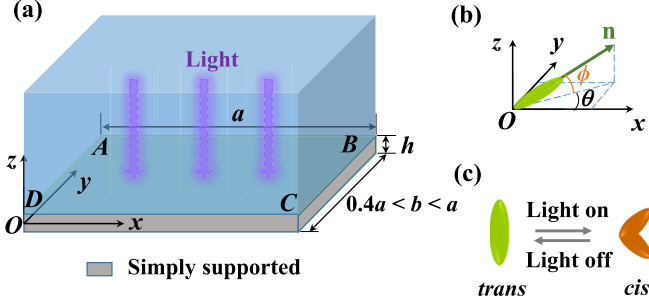
FIG. 1. (a) Sketch of a simply supported rectangular LCE plate illuminated by downward light (the width of the plate changes from 0.4 a to a); (b) the director **n** has an angle ϕ with xOy plane, and its projection in xOy plane has an angle θ with x axis; (c) the light-induced transformation between *trans* and *cis*.

governing equation of spontaneous bending for an anisotropic LCE rectangular plate has been derived as

$$d_{11}\frac{\partial^4 \bar{w}}{\partial \bar{x}^4} + 4d_{14}\frac{\partial^4 \bar{w}}{\partial \bar{x}^3 \partial \bar{y}} + 4d_{24}\frac{\partial^4 \bar{w}}{\partial \bar{x} \partial \bar{y}^3} + 2(d_{12}+2d_{44})\frac{\partial^4 \bar{w}}{\partial \bar{x}^2 \partial \bar{y}^2}$$

$$+ d_{22}\frac{\partial^4 \bar{w}}{\partial \bar{y}^4} = -\frac{\partial^2 \bar{M}_{xx}^s}{\partial \bar{x}^2} - 2\frac{\partial^2 \bar{M}_{xy}^s}{\partial \bar{x} \partial \bar{y}} - \frac{\partial^2 \bar{M}_{yy}^s}{\partial \bar{y}^2}, \quad (1)$$

where

$$\bar{M}_{xx}^s = -d_{11}\alpha\frac{\partial \gamma_{sx}}{\partial \bar{x}} - d_{14}\alpha\frac{\partial \gamma_{sx}}{\partial \bar{y}} - d_{12}\alpha\frac{\partial \gamma_{sy}}{\partial \bar{y}} - d_{14}\alpha\frac{\partial \gamma_{sy}}{\partial \bar{x}}$$

$$+ 6\alpha^2 P_{0\|}\eta_0 T_0 I_0 [2\beta^2 - \beta - (2\beta^2 + \beta)\exp(-1/\beta)]$$

$$\times [(1 + \nu_s)\cos^2\phi(d_{11}\cos^2\theta + d_{12}\sin^2\theta + d_{14}\sin 2\theta)$$

$$- \nu_s(d_{11} + d_{12})], \quad (2)$$

$$\bar{M}_{xy}^s = -d_{41}\alpha\frac{\partial \gamma_{sx}}{\partial \bar{x}} - d_{44}\alpha\frac{\partial \gamma_{sx}}{\partial \bar{y}} - d_{42}\alpha\frac{\partial \gamma_{sy}}{\partial \bar{y}} - d_{44}\alpha\frac{\partial \gamma_{sy}}{\partial \bar{x}}$$

$$+ 6\alpha^2 P_{0\|}\eta_0 T_0 I_0 [2\beta^2 - \beta - (2\beta^2 + \beta)\exp(-1/\beta)]$$

$$\times [(1 + \nu_s)\cos^2\phi(d_{41}\cos^2\theta + d_{42}\sin^2\theta + d_{44}\sin 2\theta)$$

$$- \nu_s(d_{41} + d_{42})], \quad (3)$$

$$\bar{M}_{yy}^s = -d_{21}\alpha\frac{\partial \gamma_{sx}}{\partial \bar{x}} - d_{24}\alpha\frac{\partial \gamma_{sx}}{\partial \bar{y}} - d_{22}\alpha\frac{\partial \gamma_{sy}}{\partial \bar{y}} - d_{24}\alpha\frac{\partial \gamma_{sy}}{\partial \bar{x}}$$

$$+ 6\alpha^2 P_{0\|}\eta_0 T_0 I_0 [2\beta^2 - \beta - (2\beta^2 + \beta)\exp(-1/\beta)]$$

$$\times [(1 + \nu_s)\cos^2\phi(d_{21}\cos^2\theta + d_{22}\sin^2\theta + d_{24}\sin 2\theta)$$

$$- \nu_s(d_{21} + d_{22})], \quad (4)$$

where

$$\bar{x} = \frac{x}{a}, \quad \bar{y} = \frac{y}{a}, \quad \bar{w} = \frac{w}{h}, \quad \alpha = \frac{a}{h}, \quad \beta = \frac{d_0}{h},$$

$$(d_{11}, d_{12}, d_{14})$$

$$= \left(\frac{D_{11}}{D_{11}}, \frac{D_{12}}{D_{11}}, \frac{D_{14}}{D_{11}}\right), \quad (d_{22}, d_{24}, d_{41}, d_{42}, d_{44})$$

$$= \left(\frac{D_{22}}{D_{11}}, \frac{D_{24}}{D_{11}}, \frac{D_{41}}{D_{11}}, \frac{D_{42}}{D_{11}}, \frac{D_{44}}{D_{11}}\right), \quad (5)$$

and $D_{ij} = C_{ij}h^3/12(i, j = 1, 2, 4)$, $C_{ij}(i, j = 1, 2, 4)$ are elements of material elastic matrix which are shown in Appendix A. η_0 is the light absorption constant and T_0 is the thermal characteristic time from the *cis* state to the *trans* state, I_0 is the light intensity at the upper plate surface. $P_{0\|}$ denotes the contraction coefficient which is parallel to the director **n** and ν_s is spontaneous strain ratio.

Here, the simply supporting boundary conditions are considered, and the dimensionless boundary conditions are with the form

$$(\bar{w})_{\bar{x}=0,1} = (\bar{w})_{\bar{y}=0,\zeta} = 0, \quad (6)$$

$$\left(-d_{11}\frac{\partial^2 \bar{w}}{\partial \bar{x}^2} - d_{12}\frac{\partial^2 \bar{w}}{\partial \bar{y}^2} - 2d_{14}\frac{\partial^2 \bar{w}}{\partial \bar{x} \partial \bar{y}} - \bar{M}_{xx}^s\right)_{\bar{x}=0,1} = 0,$$

$$\left(-d_{21}\frac{\partial^2 \bar{w}}{\partial \bar{x}^2} - d_{22}\frac{\partial^2 \bar{w}}{\partial \bar{y}^2} - 2d_{24}\frac{\partial^2 \bar{w}}{\partial \bar{x} \partial \bar{y}} - \bar{M}_{yy}^s\right)_{\bar{y}=0,\zeta} = 0. \quad (7)$$

Comparing with our previous work [36], the only difference is the arbitrary plate dimension ratio ζ is taken into consideration.

In order to solve Eq. (1), the plate is divided into $(m + 1)$ pieces in the x-coordinate direction and $(n + 1)$ pieces in the y-coordinate direction with step length λ, after which a divided region of $(m + 1) \times (n + 1)$ dimensions is obtained. The nodes of the plate change from $j = 1$ to $m + 2$ in the x direction and from $i = 1$ to $n + 2$ in the y direction. By using the finite-difference method, the discretization of the governing equation is obtained as

$$[6(d_{11} + d_{22})+8(d_{12} + 2d_{44})]w_{i,j} + d_{11}w_{i,j+2}$$

$$- 4(d_{11} + d_{12} + 2d_{44})w_{i,j+1} + d_{11}w_{i,j-2} + d_{24}w_{i+2,j+1}$$

$$+ d_{22}w_{i+2,j} - 4(d_{11} + d_{12} + 2d_{44})w_{i,j-1} - d_{24}w_{i+2,j-1}$$

$$- 4(d_{12} + 2d_{44} + d_{22})w_{i+1,j} - 4(d_{12} + d_{22} + 2d_{44})w_{i-1,j}$$

$$+ [2(d_{12} + 2d_{44}) - 2(d_{14} + d_{24})]w_{i+1,j+1} + d_{14}w_{i+1,j+2}$$

$$+ [2d_{14} + 2d_{24} + 2(d_{12} + 2d_{44})]w_{i+1,j-1} - d_{14}w_{i+1,j-2}$$

$$+ [2d_{14} + 2d_{24} + 2(d_{12} + 2d_{44})]w_{i-1,j+1} - d_{14}w_{i-1,j+2}$$

$$+ [-2d_{14} - 2d_{24} + 2(d_{12} + 2d_{44})]w_{i-1,j-1} + d_{22}w_{i-2,j}$$

$$- d_{24}w_{i-2,j+1} + d_{14}w_{i-1,j-2} + d_{24}w_{i-2,j-1} = 0. \quad (8)$$

As shown in Fig. 2, the values of virtual nodes can be replaced by the displacements of the nodes that are beside the boundary in the plate. The replacement procedure is shown in Appendix B. Then a set of algebraic equations with $m \times n$ unknown displacement components are expressed as

$$\mathbf{A}_{(m\times n)\times(m\times n)}\mathbf{V}_{(m\times n)\times 1} = \mathbf{B}_{(m\times n)\times 1}, \quad (9)$$

where $\mathbf{V} = \{w_{2,2}, \ldots, w_{2,m+1}, \ldots w_{n+1,2}, \ldots, w_{n+1,m+1}\}$ is the unknown dimensionless displacement components of the $m \times n$ nodes inside the plate. Then the light-induced spontaneous bending of an arbitrary LCE plate is obtained.

III. NUMERICAL RESULTS AND DISCUSSION

Based on the above scheme, the spontaneous bending configurations for simply supported LCE plates with different sizes are investigated. In the calculations, we take $E_\|/E_\perp = 2$,

(a) BC edge   **(b) AD edge**

(c) CD edge   **(d) AB edge**

• **nodes inside plate**   ▲ **virtual nodes** λ **step length**
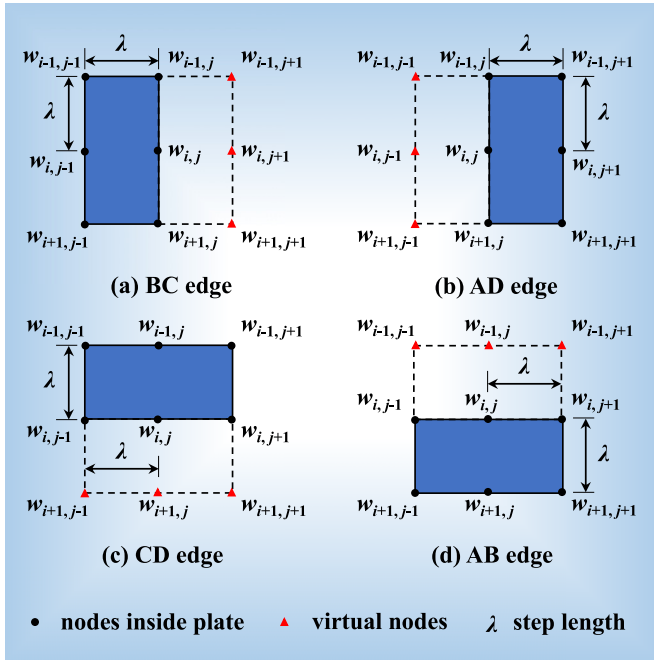
FIG. 2. The boundary conditions for simply supported LCE plate edges.

$G/E_{\parallel} = 0.1$, $V_{\parallel} = V_{\perp} = 0.5$, $T_0 = 0.4\,\text{s}$, $\eta_0 = 0.000\,22\,\text{s}^{-1}$, $P_{0\parallel} = 0.001$, $d_0 = h$, $I_0 = 10\,\text{kw}\,\text{m}^{-2}$ [32–34].

A. The effect of director orientation on the spontaneous deformation of LCE square plate

Firstly, $\zeta = 1$ is considered to study the influence of the director orientation on the spontaneous deformation of LCE square plate. Seen as Fig. 3, with the variation of director orientation, three spontaneous bending modes are observed, that is, the unimodal shape S1-1 [Fig. 3(a), the plate bends against the light direction with only one deflection maximum at the plate center], bimodal shape S2-1 [Fig. 3(b), the plate bends against the light direction with two deflection maxima], and the multimodal shape S3 [Fig. 3(c), part of the plate bends along the light direction and the other part bends against the light direction with multiple positive maxima and negative minima]. It should be noted that for Sp-q, p represents the spontaneous bending shape ($p = 1, 2, 3$, corresponds to the unimodal, bimodal, and multimodal shapes, respectively), and q represents the spontaneous bending direction ($q = 1$,

2, against or along the light direction, respectively). For the bimodal and multimodal shapes, the central area of the plate is a saddle shape. This is because the opto-Poisson effect leads to opposite strains in the directions that are along and perpendicular to the director. In addition, the constraint of the boundary condition restrains the displacement of boundary nodes, resulting in these complex deformation modes.

Figure 4 shows the contour maps for the deflection of the LCE plate under different θ and $\phi = 55°$. It is seen that the spontaneous deformation is all unimodal shape, and the deflection is central symmetric. However, the maximum deflection area (red range near the plate center in the contour map) changes with the variation of θ. When $\theta < 45°$, the red contour around the plate center is prolate ellipse with the major axis along the $\bar{y}$ axis [Figs. 4(a) and 4(b)]. When $\theta = 45°$, the central red contour changes to a circle [Fig. 4(c)]. Along with the further increase of θ, the central red contour changes again to an oblate ellipse, with the major axis along the $\bar{x}$ axis [Figs. 4(d)–4(f)]. In general, with the increasing of θ from $0°$ to $180°$, the contour of the maximum deflection area changes from prolate ellipse to oblate ellipse. $\theta = 45°$ is the critical transform angle, at which the central red contour is a circle. Moreover, it is noticed that the maximum deflections coincide with each other when the sum of director orientation θ is $90°$ or $180°$. This is induced by the symmetry of the material and the geometric symmetry of the square plate.

Figure 5 plots the contour maps for the deflection of LCE plate under different θ when $\phi = 39°$. It can be seen that with the increasing of director orientation θ, the configuration of the spontaneous bending transforms between multimodal shape and unimodal shape. The deflection is also central symmetric and the maximum deflection points of the multimodal shape are not at the plate center. When $\theta = 0°$, the contour map is a horizontal hourglass with two minimum points (blue area) at $\bar{y} = 0.5$ and two maximum points (red area) at $\bar{x} = 0.5$ [Fig. 5(a)]. When $\theta = 30°$, the contour map changes to a positive four-leaf clover shape with two maximum points at $\bar{x} = 0.5$ [Fig. 5(b)]. When $\theta = 45°$, the central red contour changes to a circle [Fig. 5(c)]. Along with the further increase of θ, the contour map changes to a minus four-leaf clover with two maximum points at $\bar{y} = 0.5$ [Fig. 5(d)]. When $\theta = 90°$, the contour map is a vertical hourglass with two minimum points at $\bar{x} = 0.5$ and two maximum points at $\bar{y} = 0.5$ [Fig. 5(e)]. Along with the increase of θ, it changes back to minus four-leaf clover [Fig. 5(f)]. It is seen that in this situation, with the increasing of θ, the contour map for four deflection peaks changes on the order of hourglass, four-leaf clover, and hour-

(a) S1-1: Unimodal   **(b) S2-1: Bimodal**   **(c) S3: Multimodal**
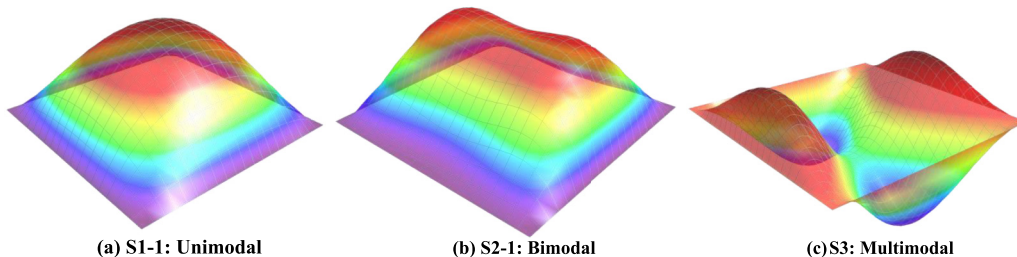
FIG. 3. The spontaneous bending configurations of the simply supported LCE square plate.
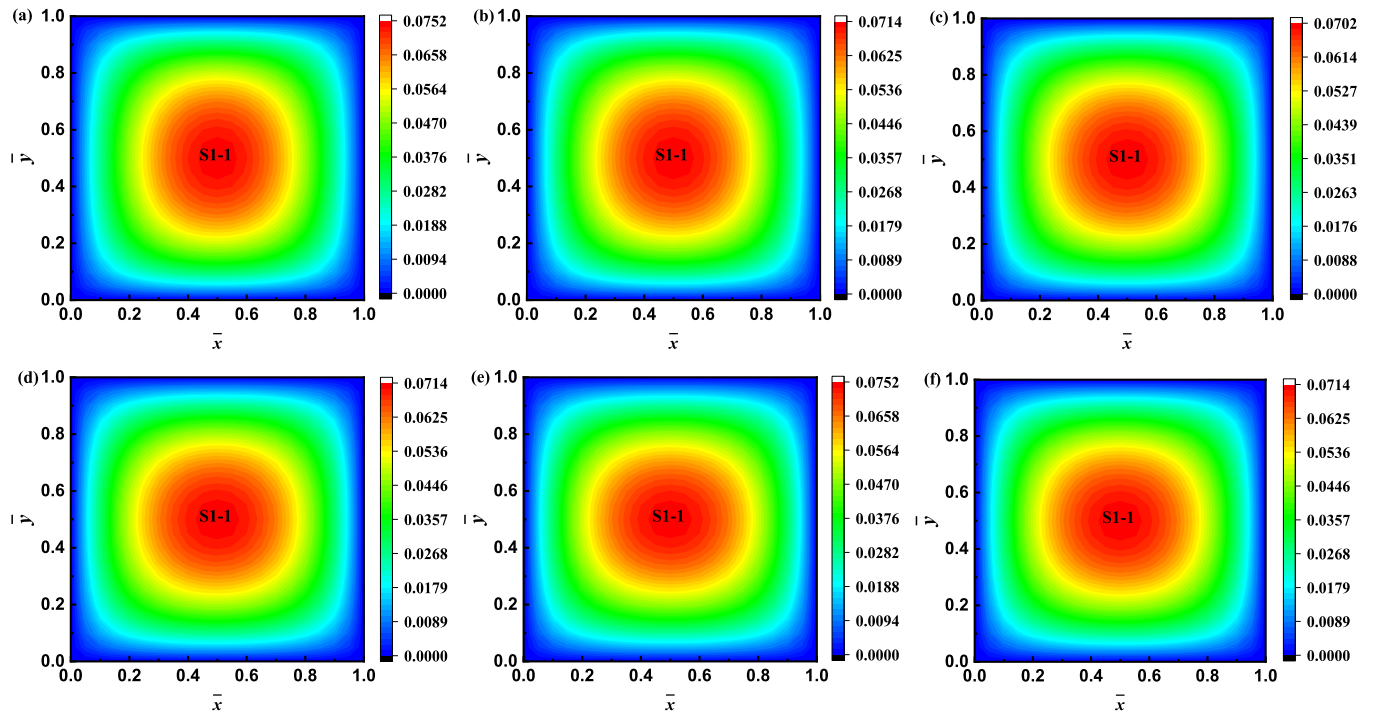
FIG. 4. The contour maps for spontaneous bending of LCE square plate with $\phi = 55°$ and (a) $\theta = 0°$ (b) $\theta = 30°$ (c) $\theta = 45°$ (d) $\theta = 60°$ (e) $\theta = 90°$ (f) $\theta = 120°$.

glass. $\theta = 45°$ is the critical transformation angle at which the contour is a circle. The hourglass or four-leaf clover change from horizontal or positive to vertical or minus, respectively. In addition, when the sum of director orientation θ is $90°$ or $180°$, the spontaneous deformation modes are of the same

kind and the maximum deflections coincide with each other. This is in accordance with that when $\phi = 55°$.

It is seen that the spontaneous bending modes are dependent on the director orientation θ and ϕ. With a vast amount of calculation, the partition of director orientation θ and ϕ
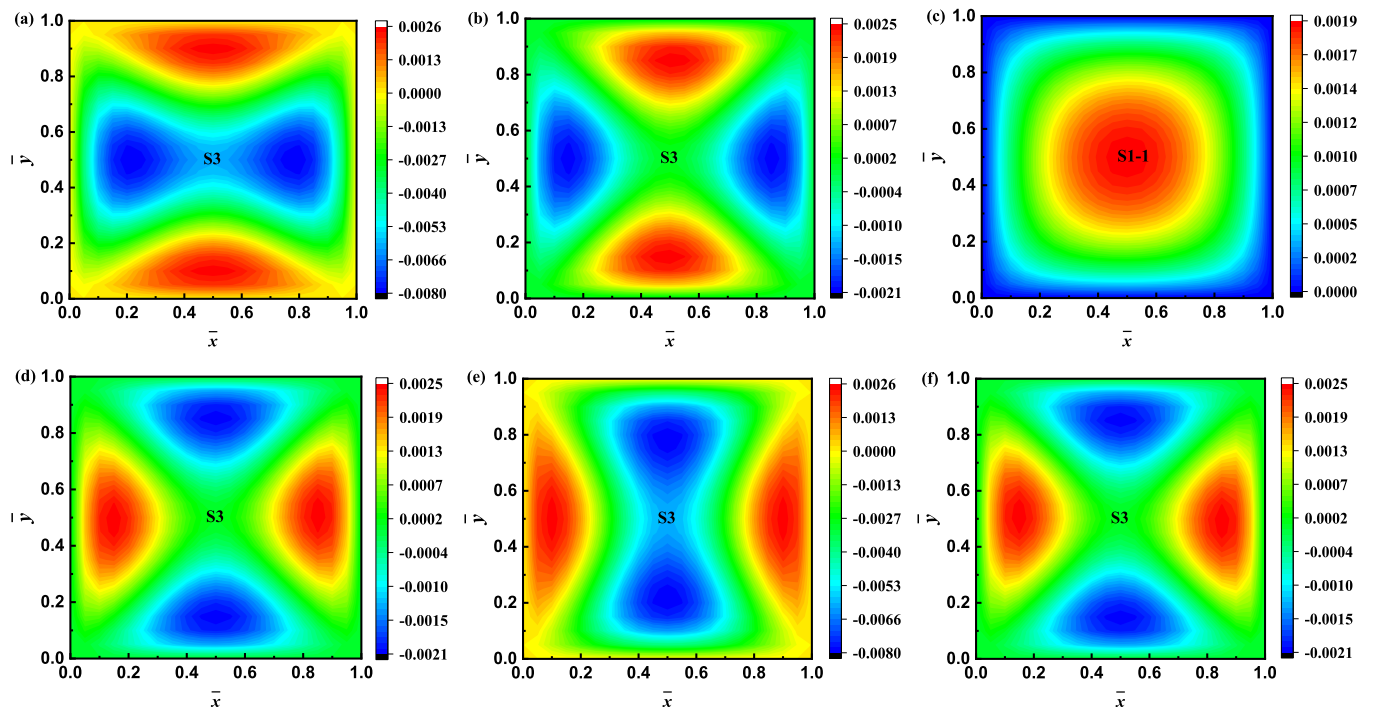
FIG. 5. The contour maps for spontaneous bending of LCE square plate with $\phi = 39°$ and (a) $\theta = 0°$ (b) $\theta = 30°$ (c) $\theta = 45°$ (d) $\theta = 60°$ (e) $\theta = 90°$ (f) $\theta = 120°$.
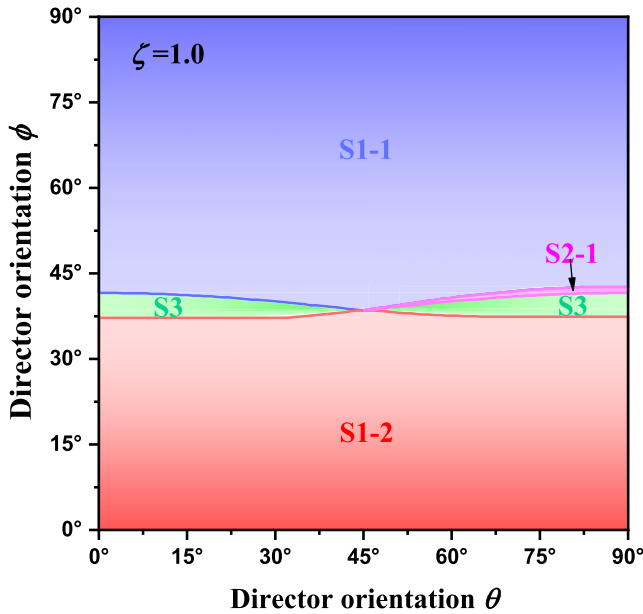
FIG. 6. The regions of director orientation θ and ϕ that lead to different spontaneous deformation modes of LCE square plate ($\zeta = 1$).

for different spontaneous deformation modes of LCE square plate are given in Fig. 6. It is seen that the deformation modes are mainly S1 or S3, whereas only in a small range S2-1

forms. It is also noticed that the spontaneous deformation mode changes symmetrically with the variation of director orientation θ and ϕ. Therefore, in the following discussion, the variation of director orientation for $0° \leqslant \theta \leqslant 90°$, and $0° \leqslant \phi \leqslant 90°$ is considered.

B. The effect of plate size on the spontaneous deformation of LCE plate

Apart from the director orientation, the plate size also has a significant influence on the deformation modes of a constrained liquid crystal elastomer plate. Comparing the above results of the square plate with those of the rectangular one ($\zeta = 0.5$) [36], it is observed that the bending modes are similar, but the division of director orientation for different spontaneous bending modes is different. Therefore, in the following part, we will further discuss the effect of the plate dimension ratio on the spontaneous deformation under a given director orientation.

Figure 7 gives the effect of the plate dimension ratio on the maximum deflection area for the simply supported LCE plate in the modes transformation process when $\theta = 90°$, $\phi = 47°$. The dashed cross lines give the maximum deflection position. It is seen that with the decreasing of the plate dimension ratio, the spontaneous bending shape changes from unimodal mode to bimodal mode. The maximum deflection area is always on the bisector of the width, and the maximum
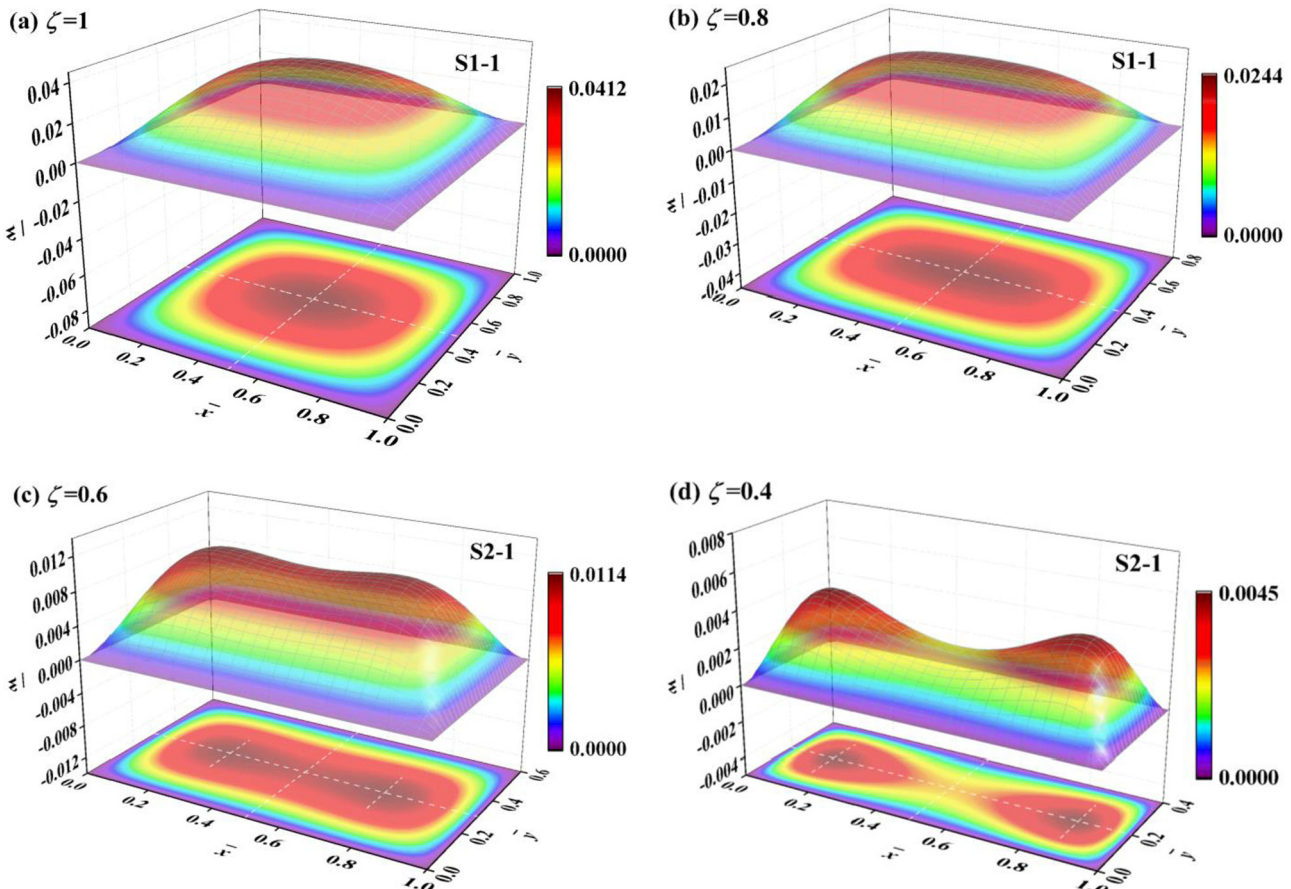
FIG. 7. The effect of plate dimension ratio on the maximum deflection area of simply supported LCE plate with $\theta = 90°$, $\phi = 47°$ (transforming from unimodal shape to bimodal shape).
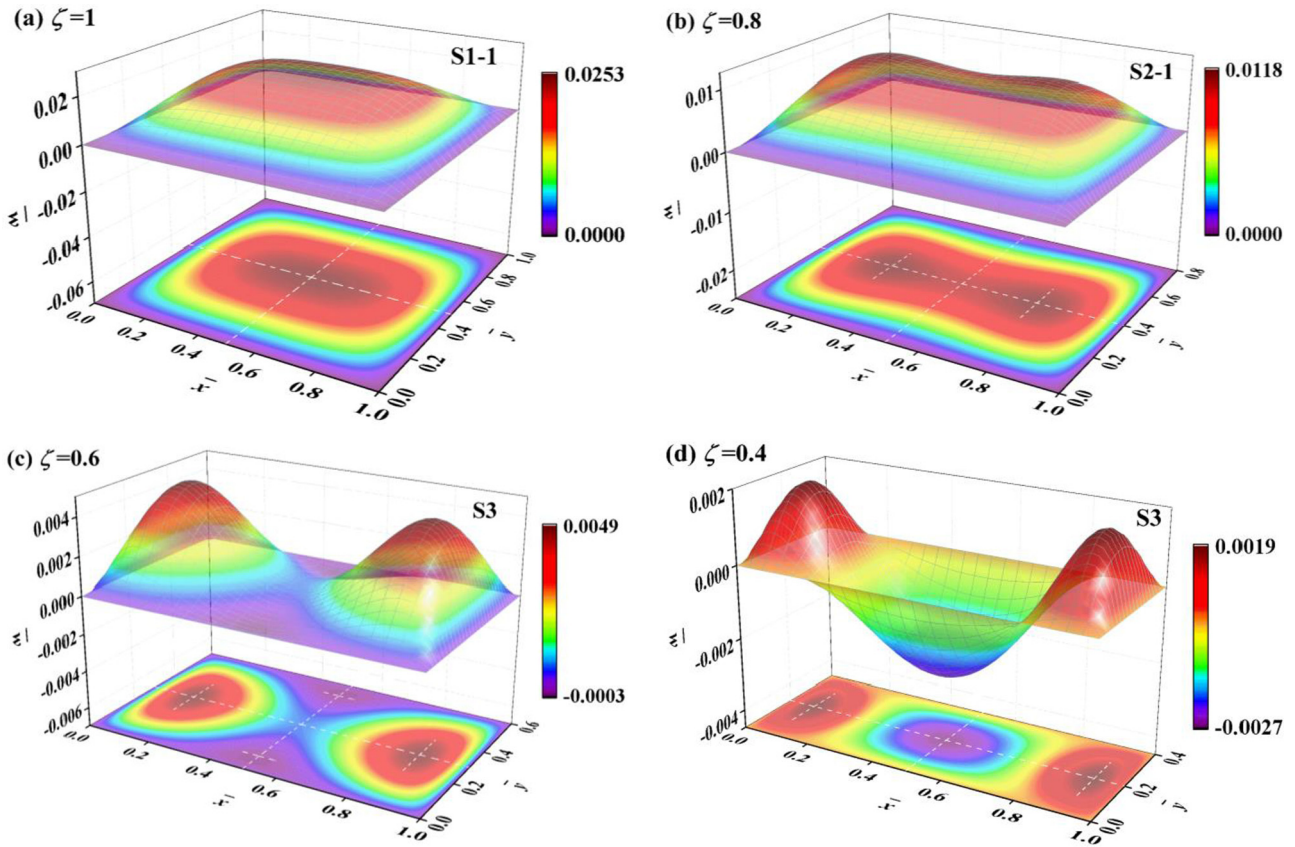
FIG. 8. The effect of the plate dimension ratio on the maximum deflection area of simply supported LCE plate with $\theta = 90°$, $\phi = 44°$ (transforming from unimodal shape to bimodal shape, and further to multimodal shape).

deflection is decreased with the decreasing of the plate dimension ratio. For the bimodal modes, the distance of the two maximum deflection areas is increased with the decreasing of ζ. This is because for a constant director orientation, the relative influence of opto-Poisson effect is increased with the decreasing of plate dimension ratio. In addition, due to the constraint of simply supported boundary condition, the spontaneous bending mode is changed with the plate size.

Figure 8 shows the effect of the plate dimension ratio on the maximum deflection area of the simply supported LCE plate in the modes transformation process when $\theta = 90°$, $\phi = 44°$. Similarly, the dashed cross lines give the maximum deflection position. It is seen that with the decreasing of plate dimension ratio, the spontaneous bending shape may change from unimodal mode to bimodal mode, and further to multimodal mode. The distance of the two positive maximum deflection areas is also increased with the decreasing of the plate dimension ratio. In addition, the positive maximum deflection is still decreased with the decreasing of the plate dimension ratio.

Figure 9 shows the effect of the plate dimension ratio on the maximum deflection area of spontaneous bending configuration of a simply supported LCE plate with $\theta = 30°$, $\phi = 40°$. With the decreasing of the plate dimension ratio, the spontaneous bending shape changes from multimodal shape to unimodal shape. The maximum deflection area is always on the bisector of the width or the length. It is seen

that with the decreasing of the plate dimension ratio, the positive maximum deflection is increased while the spontaneous bending configuration changes from multimodal shape to unimodal shape. However, the maximum deflection of unimodal is decreased with the decreasing of the plate dimension ratio.

Figure 10 gives the effect of the plate dimension ratio on the maximum deflection area of the unimodal shapes for the simply supported LCE plate when $\theta = 0°$, $\phi = 60°$. It is seen that for some director orientation, the variation of the plate dimension ratio has no effect on the bending configurations which are all unimodal shapes with the deflection maximum at the plate center. With the decreasing of the plate dimension ratio, the shape of the maximum deflection area changes from circle to ellipse, and the long axis of the ellipse will become longer. Moreover, the maximum deflection is decreased with the decreasing of the plate dimension.

It is observed that the plate size has a great influence on the spontaneous deformation of simply supported LCE plate with constant director orientation. In order to manifest this effect clearly, Fig. 11 gives the division of director orientation for spontaneous bending modes Sp-q ($p = 1, 2, 3$ and $q = 1, 2$) with different ζ. It is seen that with the decreasing of plate dimension ratio, the region for unimodal mode (S1-1 and S1-2) is decreased, whereas the regions for bimodal mode (S2-1 and S2-2) and multimodal mode (S3) are increased. This is because the influence of the boundary parallel to the
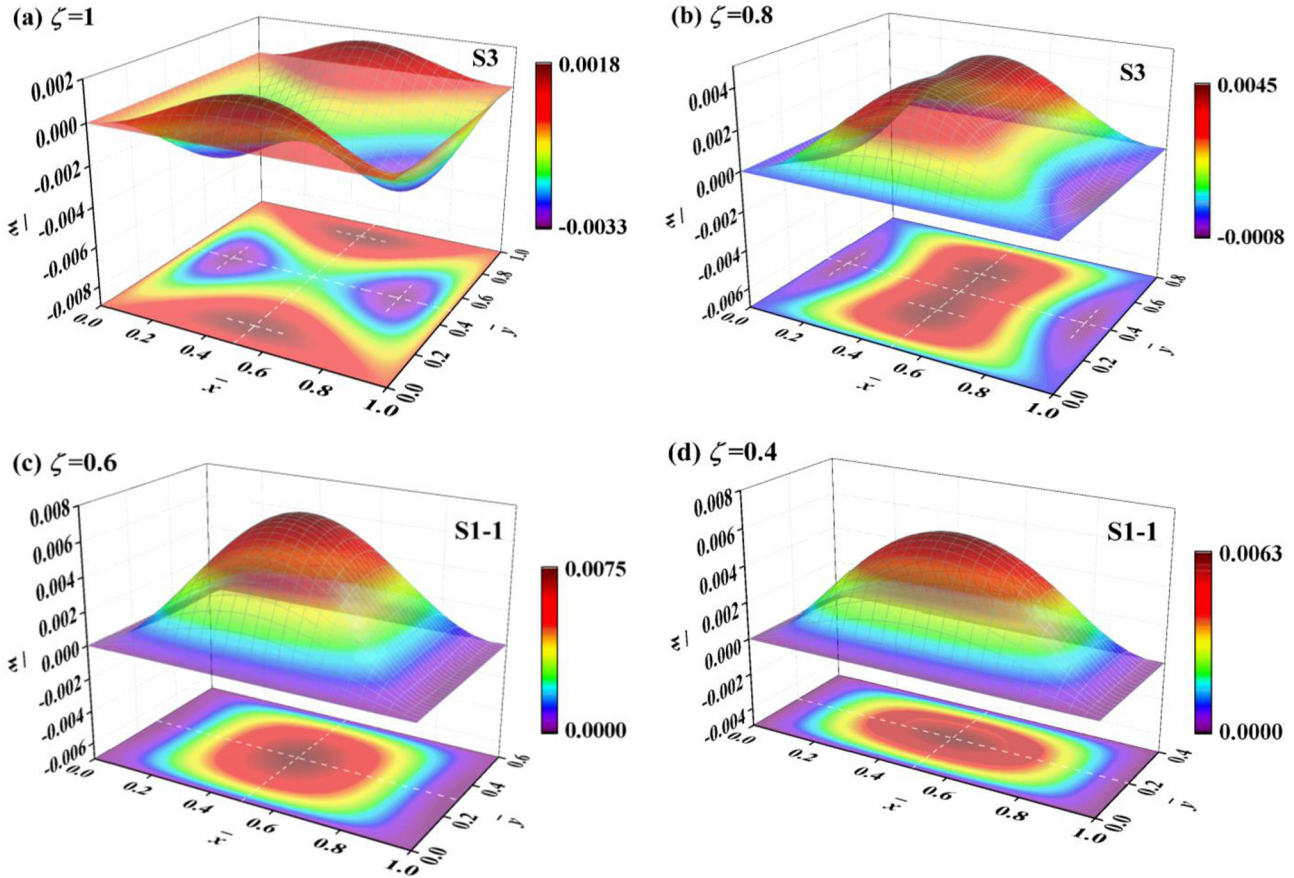
FIG. 9. The effect of the plate dimension ratio on the maximum deflection area of simply supported LCE plate with $\theta = 30°$, $\phi = 40°$ (transforming from multimodal shape to unimodal shape).

x axis is relatively enhanced with the decreasing of ζ. It is easier to obtain complex deformation in the x-axis direction, leading to larger region of bimodal and multimodal modes. As shown in Figs. 11(b) and 11(c), it is interesting to find that when the plate dimension is close to the golden ratio (between 0.61 and 0.62), the partition line between the region S1-2 and S2-2 goes through the point ($\theta = 0°$, $\phi = 0°$). As seen in Figs. 11(a)–11(c), with the decreasing of ζ, the region of ϕ for bimodal (S2-2) is extended. When ζ is larger than the golden ratio, the planar nematic with in-plane director ($\phi = 0°$) is all unimodal (S1-2). When ζ is smaller than the golden ratio, the planar nematic with in-plane director ($\phi = 0°$) will have both unimodal (S1-2) and bimodal (S2-2) modes. Moreover, the region of θ for bimodal (S2-2) is extended with the further decreasing of ζ.

IV. CONCLUSION

In this paper, the effect of plate geometry size on the spontaneous deformation of simply supported LCE plate is investigated to clarify the boundary effect. The plate size induced spontaneous bending modes transformation is clarified. Moreover, the division of director orientation and plate dimension ratio for different spontaneous bending configuration is given. From the above results, we can conclude that the following.

The director orientation and plate geometry size have a coupling effect on the spontaneous deformation of a constrained LCE plate. Three spontaneous bending modes are observed along with the variation of the director orientation or plate dimension ratio, that is, unimodal, bimodal, and multimodal shapes. With the decreasing of plate dimension ratio, the region for unimodal shape is decreased, whereas the regions for bimodal shape and multimodal shape are increased.

The maximum deflection area is always on the bisector of the width or the length. With the decreasing of plate dimension ratio, the maximum deflection of unimodal shape as well as the bimodal shape is decreased, while the distance between these two maximum deflection areas is increased. For a given director orientation, during the variation process of the plate dimension ratio, the unimodal shape has the largest maximum deflection whereas the multimodal shape has the smallest maximum deflection.

The results obtained in this paper provides a theoretical guidance on the predesign of LCE-based intelligent light-driven devices.
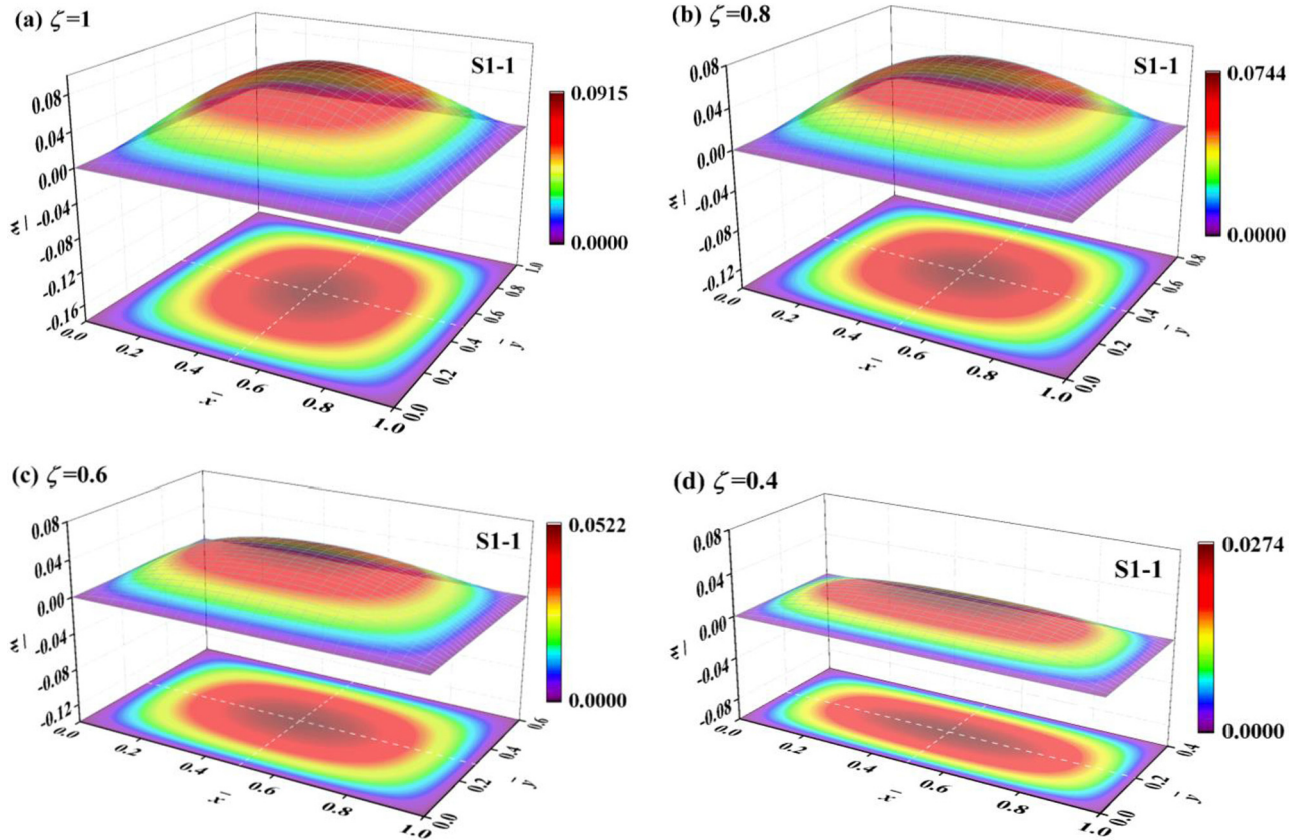
FIG. 10. The effect of the plate dimension ratio on the maximum deflection area of unimodal shape with $\theta = 0°$, $\phi = 60°$.
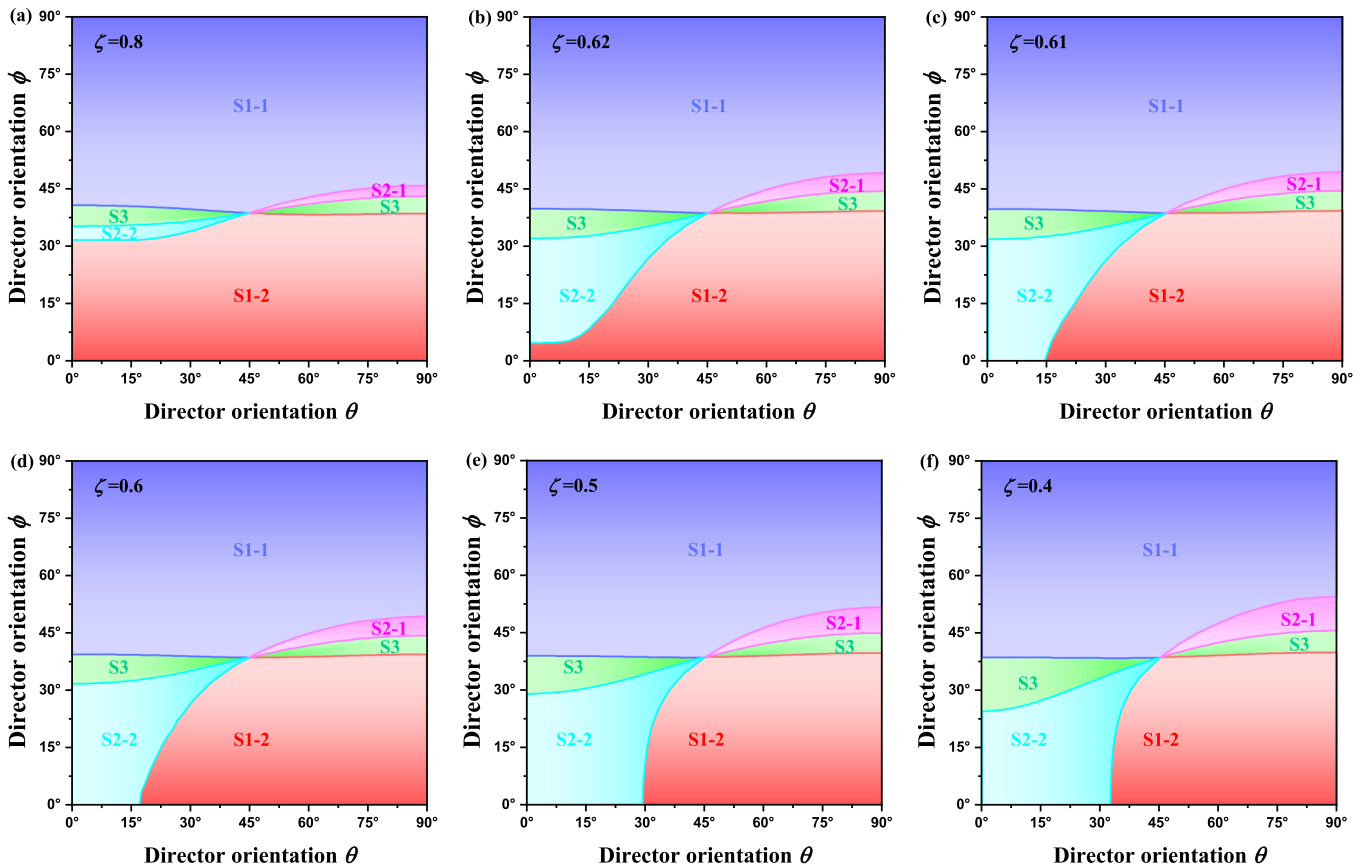
FIG. 11. The effect of the plate dimension ratio on the division for spontaneous bending configurations of the LCE plate.

APPENDIX A

The elastic matrix of the LCE plate in the given coordinate system, with the form

$$
\mathbf{C} = \mathbf{T}^{-1}
\begin{bmatrix}
C'_{11} & C'_{12} & C'_{12} & 0 & 0 & 0 \\
C'_{12} & C'_{22} & C'_{23} & 0 & 0 & 0 \\
C'_{12} & C'_{23} & C'_{22} & 0 & 0 & 0 \\
0 & 0 & 0 & C'_{44} & 0 & 0 \\
0 & 0 & 0 & 0 & C'_{22} - C'_{23} & 0 \\
0 & 0 & 0 & 0 & 0 & C'_{44}
\end{bmatrix}
(\mathbf{T}^{-1})^T,
\tag{A1}
$$

where

$$
C'_{11} = \frac{E_\parallel}{1 - s\nu_\parallel^2}, \quad
C'_{12} = \frac{E_\parallel s\nu_\parallel}{1 - s\nu_\parallel^2}, \quad
C'_{22} = \frac{E_\parallel s}{1 - s\nu_\parallel^2}, \quad
C'_{23} = \frac{E_\parallel s\nu_\perp}{1 - s\nu_\parallel^2}, \quad
C'_{44} = G.
\tag{A2}
$$

$E_\parallel$ and $E_\perp$ are the elastic modulus along and perpendicular to the director $\mathbf{n}$. $\nu_\parallel$ and $\nu_\perp$ are the Poisson ratio in the plane along and perpendicular to the director $\mathbf{n}$. G is the shear modulus and $s = E_\perp E_\parallel$. $\mathbf{T} = \mathbf{T}_2 \mathbf{T}_1$, where $\mathbf{T}_1$ and $\mathbf{T}_2$ are coordinate transform matrices with the form

$$
\mathbf{T}_1 =
\begin{bmatrix}
\cos^2\theta & \sin^2\theta & 0 & 2\cos\theta\sin\theta & 0 & 0 \\
\sin^2\theta & \cos^2\theta & 0 & -2\cos\theta\sin\theta & 0 & 0 \\
0 & 0 & 1 & 0 & 0 & 0 \\
-\cos\theta\sin\theta & \cos\theta\sin\theta & 0 & \cos^2\theta - \sin^2\theta & 0 & 0 \\
0 & 0 & 0 & 0 & \cos\theta & -\sin\theta \\
0 & 0 & 0 & 0 & \sin\theta & \cos\theta
\end{bmatrix},
\tag{A3}
$$

$$
\mathbf{T}_2 =
\begin{bmatrix}
\cos^2\phi & 0 & \sin^2\phi & 0 & 0 & 2\cos\phi\sin\phi \\
0 & 1 & 0 & 0 & 0 & 0 \\
\sin^2\phi & 0 & \cos^2\phi & 0 & 0 & -2\cos\phi\sin\phi \\
0 & 0 & 0 & \cos\phi & \sin\phi & 0 \\
0 & 0 & 0 & -\sin\phi & \cos\phi & 0 \\
-\cos\phi\sin\phi & 0 & \cos\phi\sin\phi & 0 & 0 & \cos^2\phi - \sin^2\phi
\end{bmatrix}
\tag{A4}
$$

APPENDIX B

For edge BC [as shown in Fig. 2(a), at $j = m + 2$ in the x direction and from $i = 2$ $i = 2$ to $n + 1$ in the y direction], the boundary conditions are $w = 0$ and $\bar{M}_{xx} = 0$. There,

$$
-\frac{d_{14}}{2} w_{i-1,m+1} - d_{11} w_{i,m+1} + \frac{d_{14}}{2} w_{i+1,m+1} + \frac{d_{14}}{2} w_{i-1,m+3} - d_{11} w_{i,m+3} - \frac{d_{14}}{2} w_{i+1,m+3} - \bar{M}_{xx}^s \lambda^2 = 0.
\tag{B1}
$$

Equation (B1) represents n equations when I changes from 2 to $n + 1$. Then it is written as matrix form

$$
\mathbf{A}_1 \mathbf{W} - \mathbf{A}_1^{\mathbf{F}} \mathbf{W}^{\mathbf{F}} - \bar{M}_{xx}^s \lambda^2 \mathbf{I} = 0,
\tag{B2}
$$

where $\mathbf{W}^{\mathbf{F}} = \{w_{2,m+3}, w_{3,m+3}, ..., w_{n+1,m+3}\}$ is the displacement values of virtual nodes and $\mathbf{W} = \{w_{2,m+1}, w_{3,m+1}, ..., w_{n+1,m+1}\}$ is the displacement values of the nodes that are beside the boundary in the plate. The coefficient matrices are

$$
\mathbf{A}_1 =
\begin{bmatrix}
-d_{11} & \frac{d_{14}}{2} & & & & \\
-\frac{d_{14}}{2} & -d_{11} & \frac{d_{14}}{2} & & & \\
& \cdot & \cdot & \cdot & & \\
& & \cdot & \cdot & \cdot & \\
& & & -\frac{d_{14}}{2} & -d_{11} & \frac{d_{14}}{2} \\
& & & & -\frac{d_{14}}{2} & -d_{11}
\end{bmatrix},
\tag{B3}
$$

$$
\mathbf{A}_1^{\mathbf{F}} =
\begin{bmatrix}
d_{11} & \frac{d_{14}}{2} & & & & \\
-\frac{d_{14}}{2} & d_{11} & \frac{d_{14}}{2} & & & \\
& \cdot & \cdot & \cdot & & \\
& & \cdot & \cdot & \cdot & \\
& & & -\frac{d_{14}}{2} & d_{11} & \frac{d_{14}}{2} \\
& & & & -\frac{d_{14}}{2} & d_{11}
\end{bmatrix}.
\tag{B4}
$$

Then, the values of virtual nodes ($\mathbf{W}^{\mathrm{F}} = \{w_{2,m+3}, w_{3,m+3}, ..., w_{n+1,m+3}\}$) are obtained as

$$\mathbf{W}^{\mathbf{F}} = \left(\mathbf{A}_1^{\mathrm{F}}\right)^{-1}\mathbf{A}_1\mathbf{W} - \left(\mathbf{A}_1^{\mathrm{F}}\right)^{-1}M_{xx}^s\lambda^2. \tag{B5}$$

The solving procedures for other edges are the same and not given here.

[1] M. Lahikainen, H. Zeng, and A. Priimagi, Nat Commun **9**, 4148 (2018).

[2] C. Wang *et al.* Adv. Mater. **30**, e1706695 (2018).

[3] N. An, M. Li, and J. Zhou, Smart Mater. Struct. **25**, 015016, (2016).

[4] S. Palagi, D. P. Singh, and P. Fischer, Adv. Opt. Mater. **7**, 1900370 (2019).

[5] Q. He, Z. Wang, Z. Song, and S. Cai, Adv. Mater. Technol. **4**, 1800244 (2019).

[6] H. Kajimoto and L. Jones, IEEE Trans. Haptics **12**, 257 (2019).

[7] Y. Cui, Y. Yin, C. Wang, K. Sim, Y. Li, C. Yu, and J. Song, Appl. Math. Mech. **40**, 943 (2019).

[8] S. Biswas, H. Fukushima, and L. T. Drzal, Composites, Part A **42**, 371 (2011).

[9] M. T. Brannum, A. M. Steele, M. C. Venetos, L. T. J. Korley, G. E. Wnek, and T. J. White, Adv. Opt. Mater. **7**, 1801683 (2019).

[10] Y. Shang, J. Liu, M. Zhang, W. He, X. Cao, J. Wang, T. Ikeda, and L. Jiang, Soft Matter **14**, 5547 (2018).

[11] T. J. White, *Photomechanical Materials, Composites, and Systems: Wireless Transduction of Light into Work* (John Wiley & Sons, Hoboken, NJ, 2017).

[12] M. Warner and E. M. Terentjev, *Liquid Crystal Elastomers* (Clarendon Press, Oxford, 2003), Vol. 120.

[13] J. M. Boothby, H. Kim, and T. H. Ware, Sens. Actuators, B **240**, 511 (2017).

[14] T. J. White and D. J. Broer, Nat. Mater. **14**, 1087 (2015).

[15] H. Zeng, O. M. Wani, P. Wasylczyk, and A. Priimagi, Macromol. Rapid Commun. **39**, 1700224 (2018).

[16] O. M. Wani, H. Zeng, P. Wasylczyk, and A. Priimagi, Adv. Opt. Mater. **6**, 1700949 (2018).

[17] Y. L. Yu, M. Nakano, and T. Ikeda, Nature (London) **425**, 145 (2003).

[18] P. M. Hogan, A. R. Tajbakhsh, and E. M. Terentjev, Phys. Rev. E **65**, 041720 (2002).

[19] C. L. van Oosten, K. D. Harris, C. W. Bastiaansen, and D. J. Broer, Eur. Phys. J. E: Soft Matter Biol. Phys. **23**, 329 (2007).

[20] M. L. Dunn, J. Appl. Phys. **102**, 013506 (2007).

[21] M. Warner, C. D. Modes, and D. Corbett, Proc. R. Soc. A **466**, 2975 (2010).

[22] M. Warner, C. D. Modes, and D. Corbett, Proc. R. Soc. A **466**, 3561 (2010).

[23] F. Cirak, Q. Long, K. Bhattacharya, and M. Warner, Int. J. Solids Struct. **51**, 144 (2014).

[24] C. D. Modes, K. Bhattacharya, and M. Warner, Proc. R. Soc. A **467**, 1121 (2011).

[25] Y. You, C. Xu, S. Ding, and Y. Huo, Smart Mater. Struct. **21**, 125012 (2012).

[26] M. S. Krieger and M. A. Dias, Phys. Rev. E **100**, 022701 (2019).

[27] L. H. He and D. W. Huang, Int. J. Solids Struct. **51**, 3471 (2014).

[28] C. D. Modes, M. Warner, C. L. van Oosten, and D. Corbett, Phys. Rev. E **82**, 041111 (2010).

[29] B. A. Kowalski, C. Mostajeran, N. P. Godman, M. Warner, and T. J. White, Phys. Rev. E **97**, 012504 (2018).

[30] C. Mostajeran, M. Warner, T. H. Ware, and T. J. White, Proc. R. Soc. A **472**, 20160112 (2016).

[31] L. Jin, Y. Lin, and Y. Huo, Int. J. Solids Struct. **48**, 3232 (2011).

[32] Y. Zhang and Y. Z. Huo, Int. J. Solids Struct. **136**, 168 (2018).

[33] D. Zhao and Y. Liu, Smart Mater. Struct. **28**, 075017 (2019).

[34] D. Zhao and Y. Liu, Energy **198**, 117351 (2020).

[35] S. Conti, A. DeSimone, and G. Dolzmann, J. Mech. Phys. Solids **50**, 1431 (2002).

[36] D. Zhao and Y. Liu, Phys. Rev. E **101**, 042701 (2020).